













RESEARCH ARTICLE

10.1029/2021SW002853

Ionospheric Storm Scale Index Based on High Time Resolution UPC-IonSAT Global Ionospheric Maps (IsUG)

Key Points:

- The new ionospheric storm scale, IsUG, is presented
- The IsUG is based on the high resolution and rapid UPC-IonSAT Global Ionosphere Maps (UQRG)
- Statistical analysis is carried out on a global scale from 1997 to 2014 comparing well with the available raw GNSS data based I-scale index

Qi Liu¹ , Manuel Hernández-Pajares^{1,2} , Haixia Lyu^{3,1} , Michi Nishioka⁴ , Heng Yang^{5,1} , Enric Monte-Moreno⁶ , Tamara Gulyaeva⁷ , Yannick Béniguel⁸ , Volker Wilken⁹, Germán Olivares-Pulido¹ , and Raúl Orús-Pérez¹⁰ 

¹Universitat Politècnica de Catalunya (UPC-IonSAT), Barcelona, Spain, ²Institut d'Estudis Espacials de Catalunya (IEEC), Barcelona, Spain, ³GNSS Research Center, Wuhan University, China, ⁴National Institute of Information and Communications Technology (NICT), Tokyo, Japan, ⁵School of Electronic Information and Engineering, Yangtze Normal University, Chongqing, China, ⁶Department of TSC, TALP, Universitat Politècnica de Catalunya, Barcelona, Spain, ⁷IZMIRAN, Moscow, Russia, ⁸Informatique, Electromagnétisme, Electronique, Analyse numérique (IEEA), Courbevoie, France, ⁹German Aerospace Center (DLR), Neustrelitz, Germany, ¹⁰Wave Interaction and Propagation Section (TEC-EFW) ESA ESTEC, Noordwijk, The Netherlands

Supporting Information:

Supporting Information may be found in the online version of this article.

Correspondence to:

M. Hernández-Pajares,
manuel.hernandez@upc.edu

Citation:

Liu, Q., Hernández-Pajares, M., Lyu, H., Nishioka, M., Yang, H., Monte-Moreno, E., et al. (2021). Ionospheric storm scale index based on high time resolution UPC-IonSAT global ionospheric maps (IsUG). *Space Weather*, 19, e2021SW002853. <https://doi.org/10.1029/2021SW002853>

Received 20 JUL 2021
Accepted 10 OCT 2021

Abstract The ionospheric storms have adverse effects on the radio communications, satellite communications and also the Global Navigation Satellite Systems (GNSS) application. A new Ionospheric storm Scale from Universitat Politècnica de Catalunya (UPC) Global Ionosphere Map (GIM), IsUG, is introduced for characterizing the ionospheric state on a global scale. The IsUG is based on the Vertical Total Electron Content (VTEC) derived from the continuously computed UPC Quarter-of-an-hour time resolution Rapid GIM (UQRG), taking as reference the ones during the period 1997 to 2014. It is similar to the I-scale index previously introduced, although it was over Japan and based on raw GNSS data. The dependence of the VTEC on season, local time and geographical location at each grid point of UQRG is removed by normalizing (i.e., by subtracting the mean and dividing by the corresponding standard deviation) the percentage deviation of hourly median VTEC. After validating IsUG versus I-scale, the IsUG distribution is presented and analyzed at global scale during a severe geomagnetic storm from 7 to 10 November 2004 as an example of the potentialities of the new index. The results suggest that the IsUG global map has a great potential for the scientific study of ionospheric storms from a global perspective and also for space weather warning considering the accuracy of the recently developed real-time GIMs.

Plain Language Summary The upper part of the atmosphere, the ionosphere, affects the Global Navigation Satellite Systems (GNSS) signals crossing it. Thanks to this effect, and to the worldwide coverage of GNSS receivers, it is possible to estimate the spatial and temporal distribution of free electrons at global scale (the so called Global Ionosphere Maps, GIMs). In this work we present a new application of the GIMs, as a simple and worldwide way of providing the scale of ionospheric storm (IsUG), in agreement with a previous definition based on raw localized GNSS data, and allowing its computation in real-time.

1. Introduction

Driven by the high energy inputs resulting from geomagnetic storms, the ionospheric storms contain varying electron density and have significant impacts on the society in general and on the space environment in particular, including high ionospheric correction error for trans-ionospheric radio signals, blackouts of High Frequency (HF) communication systems and disruption of Ultra High Frequency (UHF) satellite communications (Buonsanto, 1999). The evolution of ionospheric storms can be divided into positive phase (when the electron density increases) and negative phase (when the electron density decreases; Fagundes et al., 2016). It is important to identify the ionospheric conditions for the space weather warnings to mitigate the influence of ionospheric storms.

In 1960, a monthly ionospheric index was introduced in terms of a monthly mean of the ionospheric critical frequency f_0F2 measured from several stations, reflecting the average conditions of the ionosphere (Minnis & Bazzard, 1960). And the improved ionospheric index MF2 was proposed to increase the accuracy of monthly median f_0F2 estimation and long-term prediction (Mikhailov & Mikhailov, 1995; Perrone & De

© 2021. The Authors.

This is an open access article under the terms of the [Creative Commons Attribution-NonCommercial-NoDerivs License](https://creativecommons.org/licenses/by/4.0/), which permits use and distribution in any medium, provided the original work is properly cited, the use is non-commercial and no modifications or adaptations are made.

Franceschi, 1998). To represent the real-time ionospheric conditions, the ionospheric activity indices (AI) were calculated by the comparison between real-time hourly f_0F2 and median f_0F2 of the same local time for the past 30 days (Bremer et al., 2006). Afterward the degree of ionospheric disturbance, W-index, was introduced in Gulyaeva and Stanislawska (2008) in terms of the logarithm of hourly Total Electron Content (TEC) referred to the median hourly TEC for the past 27 days. In addition, the ionosphere variability index V_{σ} was obtained by moving TEC median in the preceding 15 days with variance bounds at grid points of GIM (Gulyaeva & Mannucci, 2020). In order to remove the dependence of the ionospheric state on season, local time, and geographical position, the ionospheric storm scale (I-scale) was proposed by Nishioka et al. (2017). However, the presented I-scale was based on the hourly median TEC extracted from GNSS raw observations of the Japanese regional station network only.

The Ionosphere Working Group (Iono-WG) was created in the frame of the International GNSS Service (IGS) in 1998. One of the main goals of Iono-WG was to derive GIMs with different techniques from raw GNSS observations in IONosphere map EXchange (IONEX) format by the different analysis centers, assessing and generating a combined GIM (Feltens & Schaer, 1998; Feltens, 2007; Mannucci et al., 1998; Hernández-Pajares et al., 1998, 1999, 2009; Schaer et al., 1996, 1998). The IGS GIMs provide global VTEC at grid points with the common spatial resolution of $2.5^{\circ} \times 5^{\circ}$ in latitude and longitude (Ghoddousi-Fard, 2014; Li et al., 2015; Zhang et al., 2013). The temporal resolution of IGS GIMs ranges from 15 min to 2 h (Liu, Hernández-Pajares, Lyu, et al., 2021). Among the GIMs from different IGS Ionospheric Associate Analysis Centers (IAACs), the UQRG from UPC describes the estimated VTEC from slant GNSS observation as a tomographic two-layer voxel-based model in a sun-fixed geomagnetic reference frame and estimates the VTEC of each voxel every 15 min by Kriging interpolation technique on a global scale (Hernández-Pajares et al., 1998, 1999, 2000; Orús et al., 2005). The UQRG has been proven to be one of the most accurate GIMs (Hernández-Pajares et al., 2017; Roma-Dollase et al., 2018). In particular, UQRG is able to represent realistic VTEC structures in the challenging polar regions where few GNSS stations and observations are available and the VTEC estimation is challenging (Hernández-Pajares et al., 2020).

The good performance and high temporal resolution of UQRG allow us to introduce a new ionospheric storm scale based on the definition of I-scale and historical UQRG from 1997 to 2014. The new ionospheric storm scale is able to provide in a fast and straightforward way (based on a single daily GIM file in IONEX format instead of hundreds of raw GNSS data files) for generating a realistic global map of the ionospheric storm disturbance level, which is dependent-free on season, local time, and geographic location.

2. Data and Methodology for IsUG

The hourly median VTEC at each grid point was extracted from historical UQRG with a 15-min resolution (during the period 1997–2014). Since the spatial resolution of UQRG is $2.5^{\circ} \times 5^{\circ}$ in latitude and longitude, the hourly median VTEC is derived at 5,112 grid points on a global scale. Hereafter the derived hourly VTEC is denoted as G_{TEC} . The percentage deviation of VTEC was computed to describe the current ionospheric state as indicated in previous studies (Bremer et al., 2006; Nishioka et al., 2017). The formula can be seen in Equation 1.

$$P_{TEC} = \frac{100 \times (G_{TEC} - R_{TEC})}{R_{TEC}} \quad (1)$$

where P_{TEC} is the percentage deviation of VTEC. G_{TEC} is the hourly median VTEC derived at grid points of GIM. The hourly median VTEC is the median of the five VTEC values during 1-h interval, under the GIM VTEC temporal resolution of 15 min. The hourly median VTEC is calculated every hour (for example, 0, 1, 2 UT). The median VTEC is adopted since the median value would have lower variability than a mean value. The hourly median VTEC is also chosen to mitigate the effect of extremely large or small estimated VTEC values. The R_{TEC} is the reference median value derived from the G_{TEC} at the same local time and geographic location in the past 27 days. In this way the influence of this significant period of VTEC variability (see for example Figure 22 in Hernández-Pajares et al., 2009) is removed. The 27 days window is in agreement with the solar rotation period, which has a significant impact on the VTEC variation of ionosphere (Bremer et al., 2006; Schmölter et al., 2021). Both the 27 days variation of solar radiation and the 27 days variation of geomagnetic activity caused by the solar wind and interplanetary magnetic field, have effects

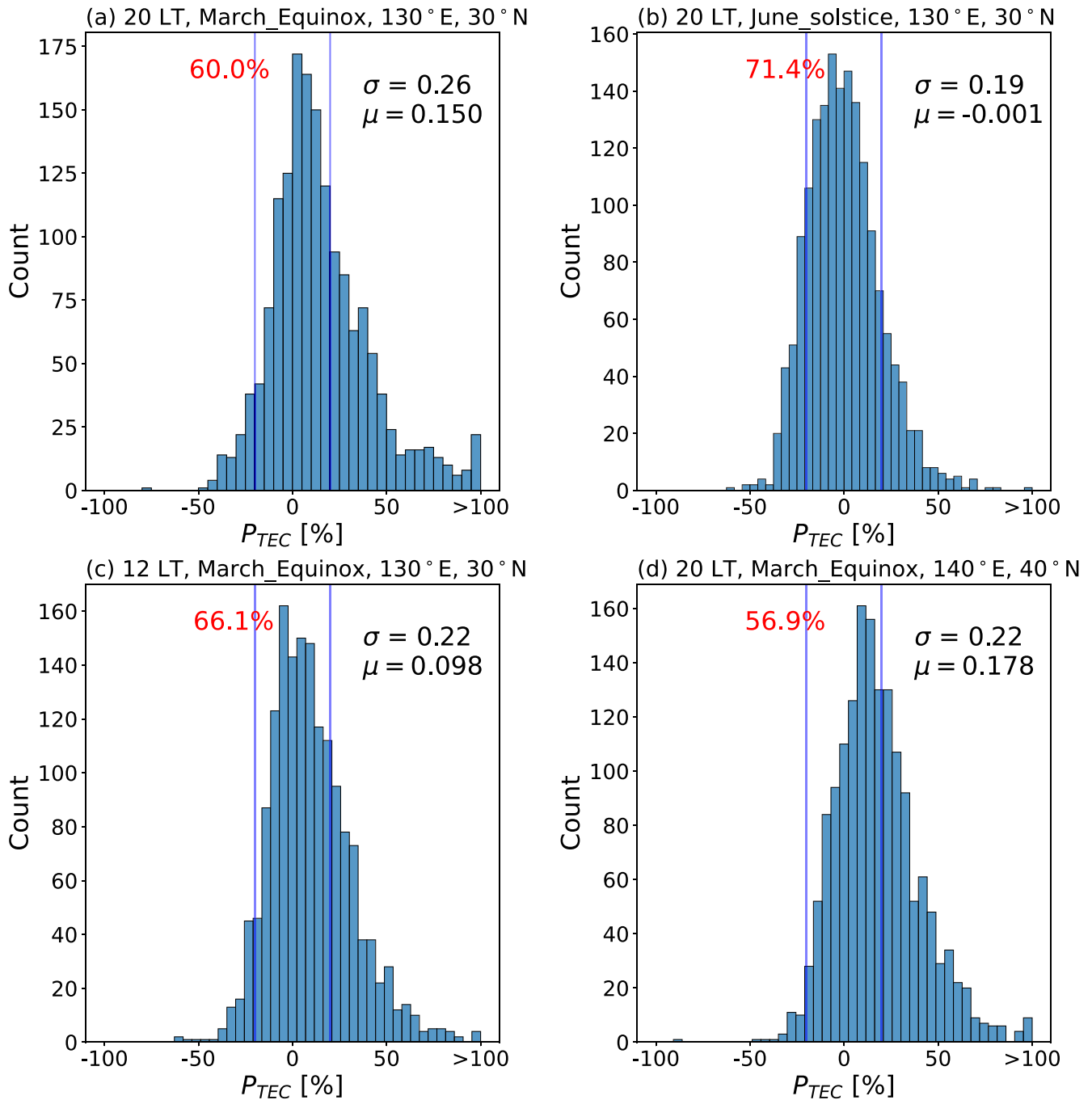


Figure 1. The distribution of P_{TEC} from 1997 to 2014 (the number in red color indicates the relative amount of the absolute percentage values $|P_{TEC}|$ below 20%). (a) P_{TEC} of (130°E, 30°N) during 3 months around March Equinox at 20 Local Time (LT) (b) P_{TEC} of (130°E, 30°N) during 3 months around June Solstice at 20 Local Time (LT) (c) P_{TEC} of (130°E, 30°N) during 3 months around March Equinox at 12 LT (d) P_{TEC} of (140°E, 40°N) during 3 months around March Equinox at 20 LT.

on ionospheric VTEC (Ma et al., 2012; Schreiber, 1998). The window size smaller and larger than 27 days is more affected by the daily variations and the seasonal variations (Nishioka et al., 2017).

With the purpose of characterizing and comparing the distribution of UQRG-GIM derived P_{TEC} at specific regions previously characterized by I-scale (Nishioka et al., 2017), the grid points of (130°E, 30°N) and (140°E, 40°N) were chosen in longitude and latitude, coinciding with the corresponding values in Nishioka

Table 1

Comparison of P_{TEC} Distribution Parameters During 1997–2014 Between the Values Derived From UQRG (Input for IsUG Index) and the Values Derived in Nishioka et al. (2017) as Input to I-Scale

Season	LT	Long.	Lat.	P_{TEC} (UQRG-GIM)			P_{TEC} (raw-GNSS-data)		
				σ	μ	per. 20%	σ	μ	per. 20%
March Equi.	20 h	130°E	30°N	0.28	0.150	60.0	0.33	0.19	54.3
June Equi.	20 h	130°E	30°N	0.19	−0.001	71.4	0.20	−0.02	69.7
March Equi.	12 h	130°E	30°N	0.22	0.098	66.1	0.26	0.08	62.1
March Equi.	20 h	140°E	40°N	0.23	0.178	56.9	0.27	0.22	50.2

et al. (2017) and the same time period (years 1997–2014). It should be noted out that the grid point of (130°E, 30°N) is within the region of 29° latitudinal band, while the grid point of (140°E, 40°N) is within the region of 41° latitudinal band as defined in Nishioka et al. (2017). In addition, the mean value μ and standard deviation σ of P_{TEC} are divided by 100 (i.e., not in %) in all the figures and tables, in order to compare with the figures and tables of Nishioka et al. (2017).

As it can be seen in Figure 1, the histograms are dissimilar at different local time, season and geographical locations. Figure 1a shows the histogram of P_{TEC} , where 60% of absolute percentage values $|P_{TEC}|$ have a value lower than 20% and can be regarded as undisturbed at grid point [130°E, 30°N]. 71.4% of absolute percentage values $|P_{TEC}|$ are lower than 20% in Figure 1b. In addition, the standard deviation σ of P_{TEC} is 0.28 and the mean value μ of P_{TEC} is 0.19 in Figure 1a, while the σ and μ of Figure 1b are 0.19 and −0.001, respectively. The difference between Figures 1a and 1b is the season: the season is March Equinox in Figure 1a, while the season is June Solstice in Figure 1b. Consequently, the P_{TEC} is affected by the season variation. In addition, the difference between Figures 1a and 1c indicates the local time dependence of P_{TEC} . In Figure 1d, 56.9% of absolute percentage values $|P_{TEC}|$ are smaller than 20% at grid point [140°E, 40°N]. These results are similar to the corresponding input P_{TEC} values for I-scale shown in Figure 1 of Nishioka et al. (2017), as it is summarized in Table 1.

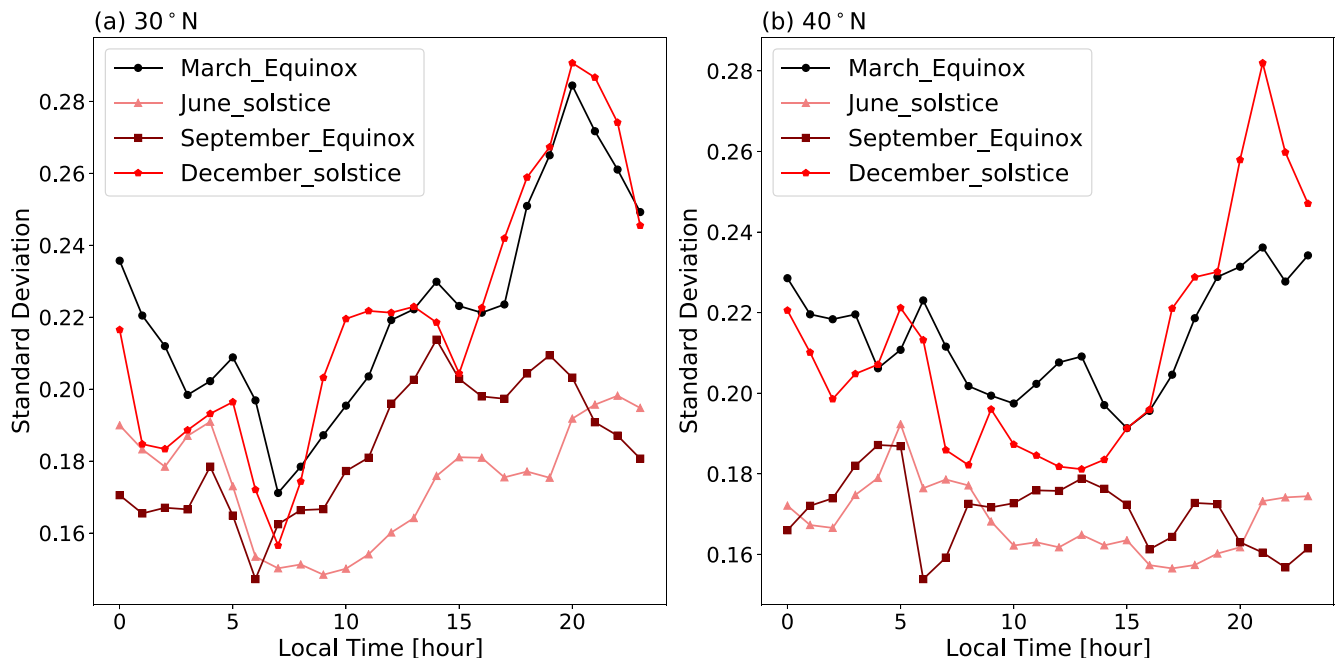


Figure 2. The variation of standard deviation at different seasons. (a) Standard deviation of (140°E, 40°N) during the period from 1997 to 2014. (b) Standard deviation of (130°E, 30°N) during the period from 1997 to 2014.

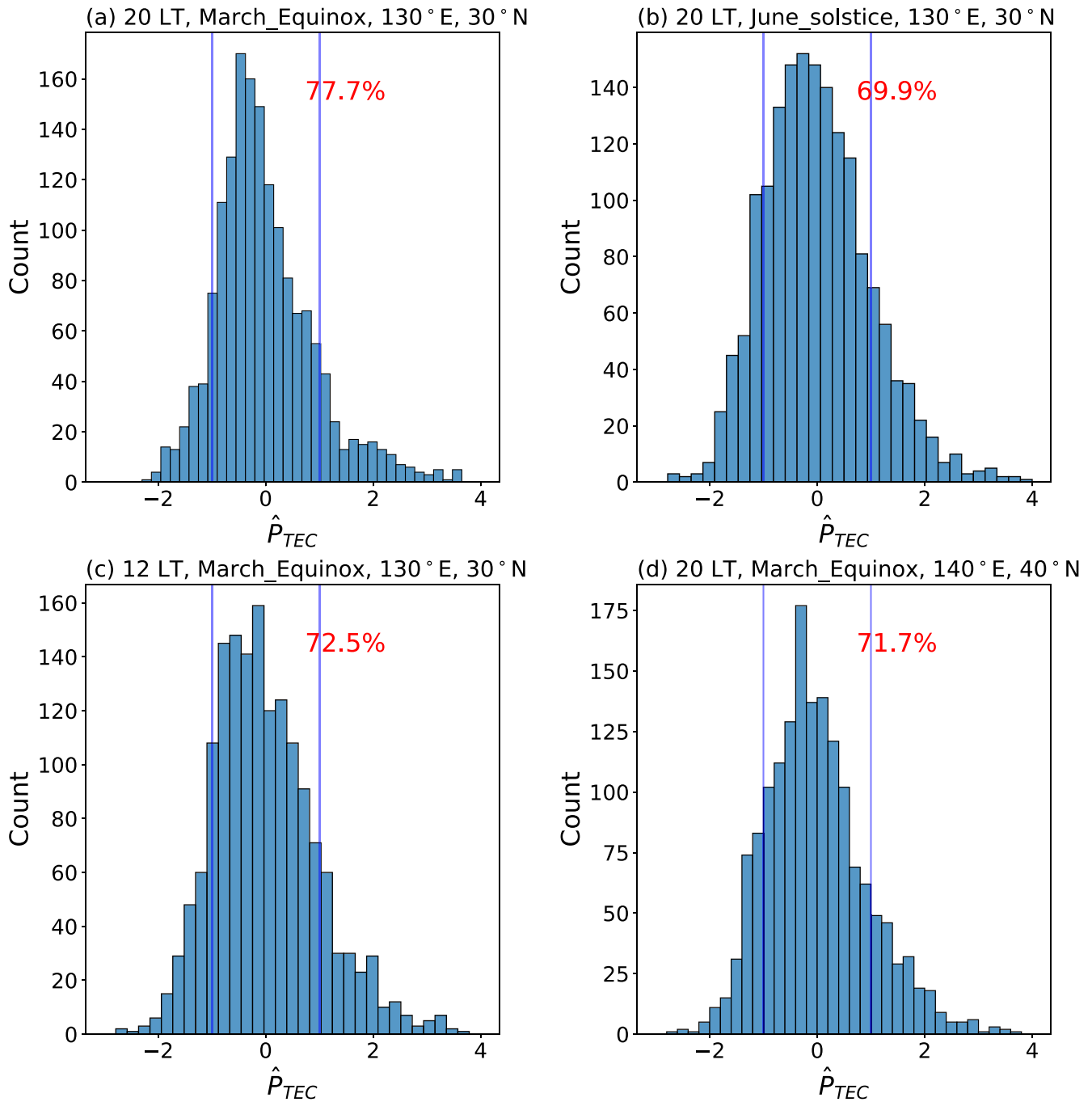


Figure 3. The distribution of \hat{P}_{TEC} from 1997 to 2014 (the number in red color indicates the rate of count when the absolute percentage values $|\hat{P}_{TEC}|$ are lower than 20%). (a) \hat{P}_{TEC} of (130°E, 30°N) during 3 months around March Equinox at 20 Local Time (LT) (b) \hat{P}_{TEC} of (130°E, 30°N) during 3 months around June Solstice at 20 LT (c) \hat{P}_{TEC} of (130°E, 30°N) during 3 months around March Equinox at 12 LT (d) \hat{P}_{TEC} of (140°E, 40°N) during 3 months around March Equinox at 20 LT.

In Figure 2a and 2b, it is shown that the standard deviation values of March Equinox and December Solstice are typically larger than the standard deviation of September Equinox and June Solstice. While the standard deviation reaches higher value around 5 and 20 local hour in Figures 2a and 2b, the standard deviation of grid point (140°E, 40°N) tends to be smoother than the grid point (130°E, 30°N) during the daytime. The LT evolution of the P_{TEC} (UQRG-GIM) standard deviation is in general similar but slightly lower when it is

Table 2

Comparison of the Percentiles for $|\hat{P}_{TEC}| \leq 1$ During 1997–2014 Between the Values Derived From UQRG (Input for IsUG Index) and the Values Derived in Nishioka et al. (2017) as Input to I-Scale

Season	LT	Long.	Lat.	\hat{P}_{TEC} (UQRG-GIM)	\hat{P}_{TEC} (raw-GNSS-data)
				(this work)	(Nishioka et al., 2017)
				perc. $ \hat{P}_{TEC} \leq 1$	perc. $ \hat{P}_{TEC} \leq 1$
March Equi.	20 h	130°E	30°N	77.7	77.5
June Equi.	20 h	130°E	30°N	69.7	72.9
March Equi.	12 h	130°E	30°N	72.5	72.6
March Equi.	20 h	140°E	40°N	71.7	72.3

compared with the corresponding results, shown in Figure 2 of Nishioka et al. (2017), but obtained from the raw-GNSS data. This is in agreement with the fact that the VTEC values provided under the GIM resolution can be smoother than the ones provided directly by the raw GNSS data.

The normalized P_{TEC} as Equation 2 is introduced to remove the dependence of P_{TEC} on season, local time and geographical location as shown in Figures 1 and 2. It should be noted that the normalized P_{TEC} is calculated at each grid point with corresponding mean value and standard deviation from 1997 to 2014.

$$\hat{P}_{TEC} = \frac{P_{TEC} - \mu}{\sigma} \quad (2)$$

where the μ and σ are the mean value and standard deviation derived from Equation 1 and shown in Figure 2. The mean value μ and standard deviation σ of P_{TEC} at each grid point are calculated every hour (in local time) during each given season.

After the normalization of P_{TEC} , 69.9% – 77.7% of absolute percentage values $|\hat{P}_{TEC}|$ are smaller than 1 in Figure 3, implying the minor difference among different season, local time, geographical location when $|\hat{P}_{TEC}| < 1$, also in agreement with the corresponding \hat{P}_{TEC} input for I-scale shown in Figure 3 of Nishioka et al. (2017). The summary of both distributions of \hat{P}_{TEC} can be seen in Table 2.

As shown in Table 3, the definition of IsUG can be seen in the first, second and third columns, for severe, strong, moderate (positive and negative) among quiet states. And the occurrence probability of IsUG at global scale is given in the fourth column. The probability of a quiet ionospheric state is 73.96%, which is similar to the I-scale results at 29°N over Japan (Table 1 in Nishioka et al., 2017). And the probabilities of either positive and negative moderate, strong, severe ionospheric storms are around 10%, 1%, 0.1%.

3. Results and Analysis

In this section, the results of IsUG based on UQRG from 1997 to 2014 are presented in detail and analyzed.

3.1. The Statistics of IsUG During a Severe Geomagnetic Storm

The consistency between the IsUG and I-scale indices can be seen in detail during geomagnetic storms. Indeed, a severe geomagnetic storm happened from November 7 to 10, 2004, as reported in previous studies (e.g., Maruyama, 2006; Maruyama et al., 2013; Sori et al., 2019). As depicted in Figure 4, the observed VTEC at [130°E, 30°N], G_{TEC} , reaches ~100 TEC Units (TECU) when the Dst value is –374 nT and the Kp value is 9– at 7 UT of November 8. And the highest \hat{P}_{TEC} (18.92) is obtained at 10 UT of November 8, as indicated as the left downward arrow in Figure 4b, taking into account the time dependence of the reference VTEC, R_{TEC} . As can be seen in Figure 5, the snapshots of UQRG VTEC, P_{TEC} , mean value μ

Table 3

The Definition and Occurrence Probability of IsUG Derived From UQRG During the Period 1997–2014

IsUG	Description	Definition	Probability on a global scale (%)
IP3	Severe positive storm	$5 < \hat{P}$	0.17
IP2	Strong positive storm	$3 < \hat{P} \leq 5$	0.72
IP1	Moderate positive storm	$1 < \hat{P} \leq 3$	12.43
I0	Quiet	$-1 < \hat{P} \leq 1$	73.96
IN1	Moderate negative storm	$-2 < \hat{P} \leq -1$	11.72
IN2	Strong negative storm	$-3 < \hat{P} \leq -2$	0.95
IN3	Severe negative storm	$\hat{P} < -3$	0.06

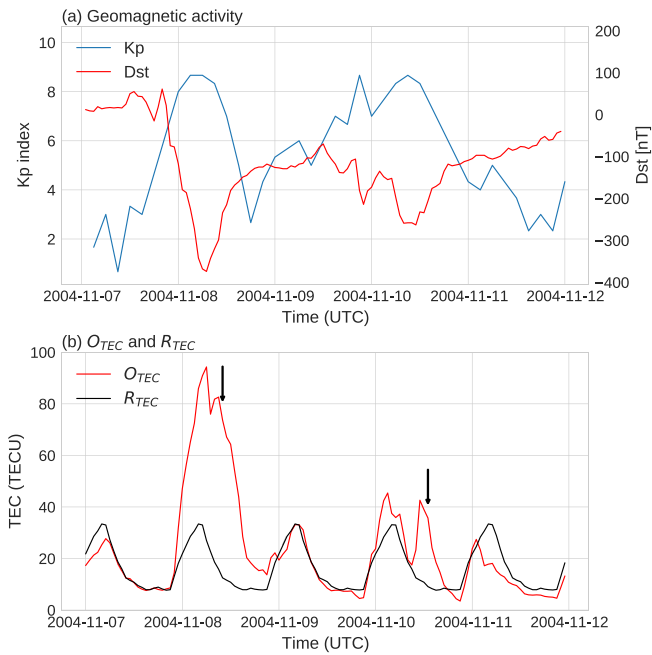


Figure 4. The evolution of G_{TEC} , R_{TEC} , Kp and Dst at (130°E, 30°N) from November 7 to 10, 2004.

of P_{TEC} and standard deviation σ of P_{TEC} at each grid point are consistent with Figure 4 when the highest \hat{P}_{TEC} (18.92) at (130°E, 30°N) is obtained. The UQRG TEC reached a high value around grid point (130°E, 30°N). It should be noted that the high value of P_{TEC} around (155°E, 30°N) is caused by high G_{TEC} (33.4) and low R_{TEC} (2.7) around 23 LT during the nighttime.

The intense TEC enhancement that might be related to the storm-induced plasma stream, has been indicated by Maruyama et al. (2013). And right downward arrow in Figure 4b indicates the second peak \hat{P}_{TEC} at 13 UT of November 10. Finally we observe that the G_{TEC} and R_{TEC} values obtained from the UQRG GIM (bottom plot of Figure 4) are almost identical to the corresponding values obtained from raw GNSS measurements (central plot of Figure 4 in Nishioka et al., 2017).

3.2. Global Map of IsUG

With the \hat{P}_{TEC} calculated at each grid point of UQRG from 1997 to 2014, the global map of IsUG can be also obtained in a straightforward way (one advantage of IsUG vs. I-scale). The detailed animations of IsUG during one quiet and one disturbed period of 2004 are presented in the Supporting Information S1.

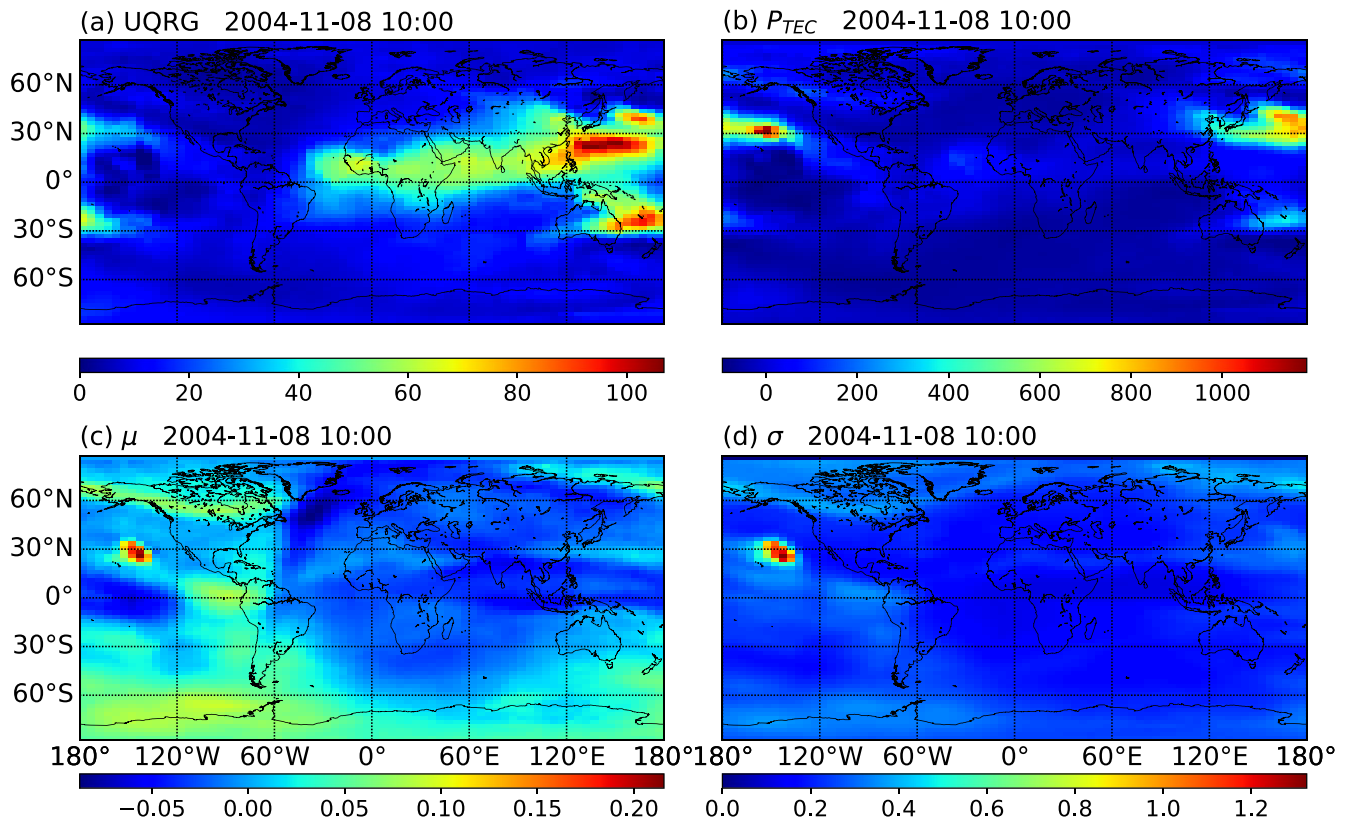


Figure 5. The snapshots of 10 UT on November 8, 2004. (a) The snapshot of UQRG VTEC (in TECU) at each grid point. (b) The snapshot of P_{TEC} value calculated by Equation 1 at each grid point. (c) The snapshot of mean value μ of P_{TEC} at each grid point. (d) The snapshot of standard deviation σ of P_{TEC} at each grid point.

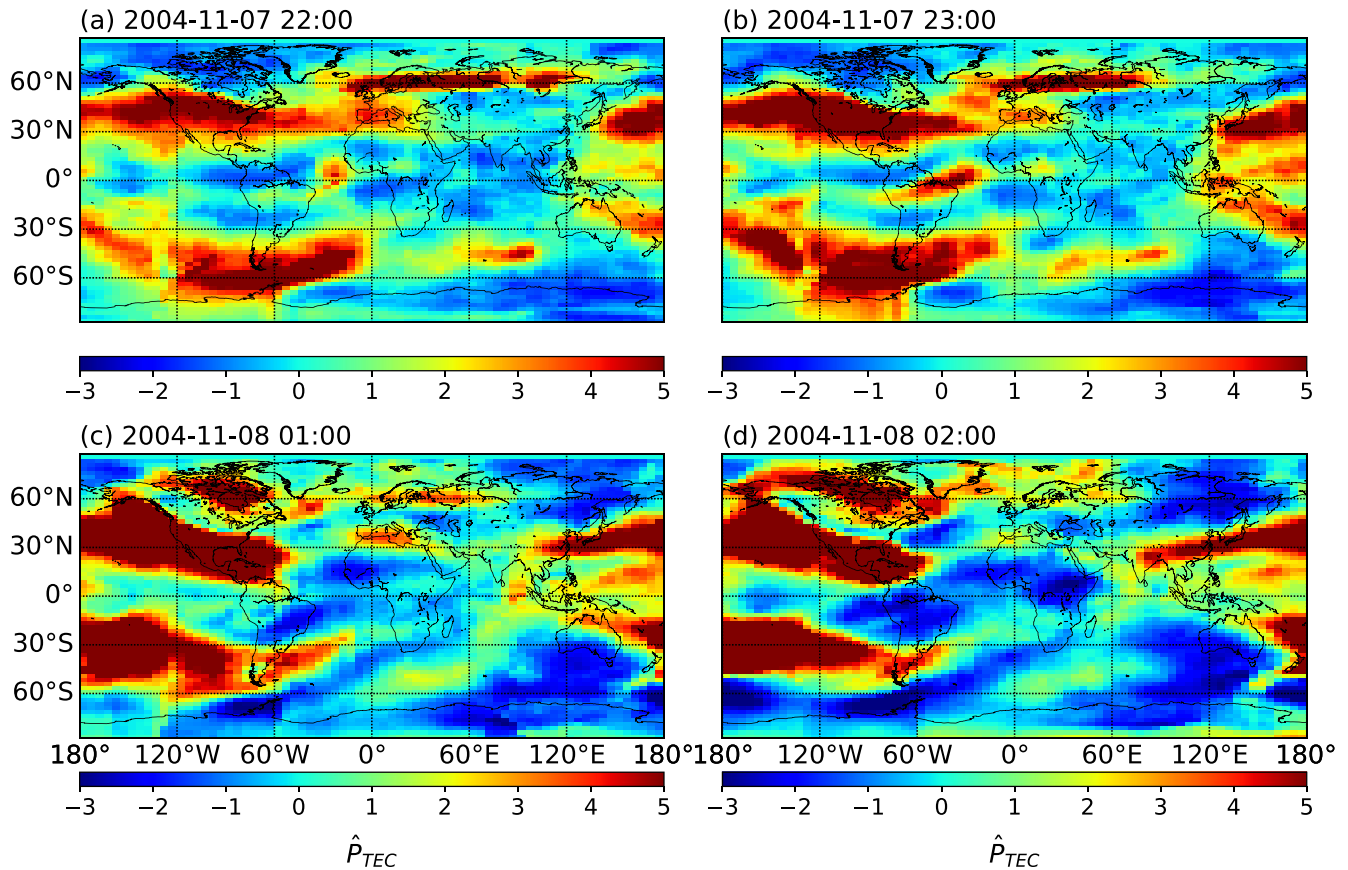


Figure 6. The IsUG global map of November 7, 8, 2004.

With a focus on specific regions, Figures 6 and 7 are selected during the severe geomagnetic storm from 7 to 10 November in 2004, which G_{TEC} (and R_{TEC}) have been previously compared and discussed over Japan.

As presented in Figure 4 and previous studies (e.g., Maruyama, 2006; Maruyama et al., 2013; Nishioka et al., 2017), the strong TEC enhancement started from 23 UT of November 7 at Japan. The enhanced TEC is coincident with the movement of severe ionospheric positive storm ($\hat{P}_{TEC} > 5$) at Japan in Figures 6a and 6b. In addition, noticeable TEC enhancement was found in a GNSS station ($77.9^{\circ}S$, $166.8^{\circ}E$) located at Antarctica (Sulaiman et al., 2007). And the TEC enhancement around the GNSS station can be also seen in the right bottom corner ($77.9^{\circ}S$, $166.8^{\circ}E$) of Figures 6c and 6d.

As shown in Figure 7a–7f, the \hat{P}_{TEC} started to increase since 14 UT and gradually expanded toward low latitude in Europe. The \hat{P}_{TEC} reached 2 (moderate positive storm) at 17 UT and 5 (severe positive storm) at 19 UT, which is consistent with the reported TEC variation in Sori et al. (2019).

4. Conclusions

From the distribution of VTEC values during the period 1997–2014 extracted from UQRG GIMs computed on a daily basis by UPC-IonSAT for IGS, the IsUG storm index is derived, extending in a straightforward way the I-scale index on a global level. The IsUG global maps are initially compared with previous studies during the severe geomagnetic storm, with a focus on the regions of Japan, Antarctica, Europe. The variation of IsUG global maps is consistent with the results of previous studies, especially over Japan (Nishioka et al., 2017) and in the Antarctica region where few GNSS stations are available (Maruyama et al., 2013; Sori et al., 2019; Sulaiman et al., 2007). Since the IGS real-time GIMs (RT-GIMs) are availability and the accuracy of RT-GIMs is presently close to the accuracy of the UQRG GIMs, the generation of real-time

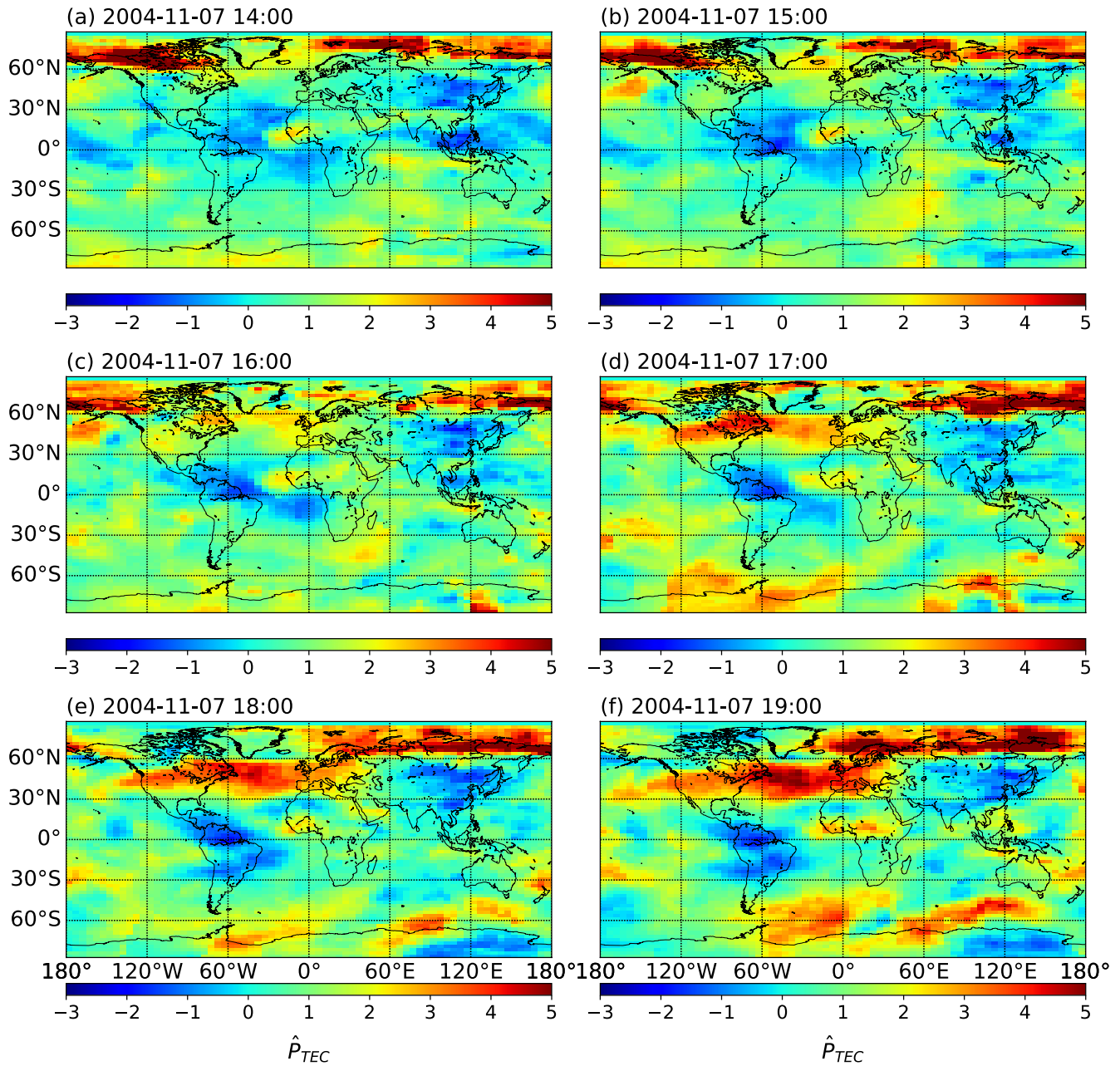


Figure 7. The IsUG global map from 14:00 to 19:00 UTC of November 7, 2004.

IsUG might be the next step (Liu, Hernández-Pajares, Yang, et al., 2021; Yang et al., 2021). In addition, the real-time ionospheric storm warning system based on real-time IsUG might be also available for space weather monitoring.

Data Availability Statement

The UQRG data are openly accessible (<https://cdis.nasa.gov/archive/gnss/products/ionex>) from Crustal Dynamics Data Information System (Noll, 2010). The Kp index is available (ftp://ftp.gfz-potsdam.de/pub/home/obs/Kp_ap_Ap_SN_F107) from GeoForschungsZentrum (Matzka et al., 2021) and Dst index is accessible (<http://wdc.kugi.kyoto-u.ac.jp/dstdir/>) from World Data Center for Geomagnetism, Kyoto (World Data Center for Geomagnetism et al., 2015).

Acknowledgments

The first author is grateful for the financial support of the China Scholarship Council (CSC). This research has been done under the partial support of the European Space Agency and European Commission funded eMON-ITOR/MoNEWIC (H2020-ESA-037) project and the European Commission funded PITHIA-NRF (H2020-INFRAIA-2018-2020 101007599) project.

References

- Bremer, J., Cander, Lj. R., Mielich, J., & Stamper, R. (2006). Derivation and test of ionospheric activity indices from real-time ionosonde observations in the European region. *Journal of Atmospheric and Solar-Terrestrial Physics*, 68(18), 2075–2090. <https://doi.org/10.1016/j.jastp.2006.07.003>
- Buonsanto, M. J. (1999). Ionospheric storms—A review. *Space Science Reviews*, 88, 563–601. <https://doi.org/10.1023/a:1005107532631>
- Fagundes, P. R., Cardoso, F., Fejer, B., Venkatesh, K., Ribeiro, B., & Pillat, V. (2016). Positive and negative GPS-TEC ionospheric storm effects during the extreme space weather event of March 2015 over the Brazilian sector. *Journal of Geophysical Research: Space Physics*, 121(6), 5613–5625. <https://doi.org/10.1002/2015ja022214>
- Feltens, J. (2007). Development of a new three-dimensional mathematical ionosphere model at European Space Agency/European Space Operations Centre. *Space Weather*, 5(12), S12002. <https://doi.org/10.1029/2006sw000294>
- Feltens, J., & Schaer, S. (1998). IGS products for the ionosphere. In *Proceedings of the 1998 IGS analysis*. Center Workshop Darmstadt.
- Ghoddousi-Fard, R. (2014). GPS ionospheric mapping at Natural Resources Canada. In *IGS workshop*.
- Gulyaeva, T., & Stanislawska, I. (2008). Derivation of a planetary ionospheric storm index. *Annales Geophysicae*, 26(9), 2645–2648. <https://doi.org/10.5194/angeo-26-2645-2008>
- Gulyaeva, T. L., & Mannucci, A. J. (2020). Echo of ring current storms in the ionosphere. *Journal of Atmospheric and Solar-Terrestrial Physics*, 205, 105300. <https://doi.org/10.1016/j.jastp.2020.105300>
- Hernández-Pajares, M., Juan, J., Sanz, J., & Solé, J. (1998). Global observation of the ionospheric electronic response to solar events using ground and LEO GPS data. *Journal of Geophysical Research*, 103(A9), 20789–20796. <https://doi.org/10.1029/98ja01272>
- Hernández-Pajares, M., Juan, J., & Sanz, J. (1999). New approaches in global ionospheric determination using ground GPS data. *Journal of Atmospheric and Solar-Terrestrial Physics*, 61(16), 1237–1247. [https://doi.org/10.1016/s1364-6826\(99\)00054-1](https://doi.org/10.1016/s1364-6826(99)00054-1)
- Hernández-Pajares, M., Juan, J., Sanz, J., & Colombo, O. L. (2000). Application of ionospheric tomography to real-time GPS carrier-phase ambiguities Resolution, at scales of 400–1000 km and with high geomagnetic activity. *Geophysical Research Letters*, 27(13), 2009–2012. <https://doi.org/10.1029/1999GL011239>
- Hernández-Pajares, M., Juan, J. M., Sanz, J., Orus, R., García-Rigo, A., Feltens, J., & Krankowski, A. (2009). The IGS VTEC maps: A reliable source of ionospheric information since 1998. *Journal of Geodesy*, 83, 263–275. <https://doi.org/10.1007/s00190-008-0266-1>
- Hernández-Pajares, M., Lyu, H., Aragón-Ángel, Á., Monte-Moreno, E., Liu, J., An, J., & Jiang, H. (2020). Polar electron content from GPS data-based global ionospheric maps: Assessment, case studies, and climatology. *Journal of Geophysical Research: Space Physics*, 125(6), e2019JA027677. <https://doi.org/10.1029/2019JA027677>
- Hernández-Pajares, M., Roma-Dollase, D., Krankowski, A., García-Rigo, A., & Orús-Pérez, R. (2017). Methodology and consistency of slant and vertical assessments for ionospheric electron content models. *Journal of Geodesy*, 91, 1405–1414. <https://doi.org/10.1007/s00190-017-1032-z>
- Li, Z., Yuan, Y., Wang, N., Hernandez-Pajares, M., & Huo, X. (2015). SHPTS: Towards a new method for generating precise global ionospheric TEC map based on spherical harmonic and generalized trigonometric series functions. *Journal of Geodesy*, 89(4), 331–345. <https://doi.org/10.1007/s00190-014-0778-9>
- Liu, Q., Hernández-Pajares, M., Lyu, H., & Goss, A. (2021). Influence of temporal resolution on the performance of global ionospheric maps. *Journal of Geodesy*, 95, 34. <https://doi.org/10.1007/s00190-021-01483-y>
- Liu, Q., Hernández-Pajares, M., Yang, H., Monte-Moreno, E., Roma-Dollase, D., García-Rigo, A., et al. (2021). The cooperative IGS RT-GIMs: A reliable estimation of the global ionospheric electron content distribution in real time. *Earth System Science Data*, 13(9), 4567–4582. <https://doi.org/10.5194/essd-13-4567-2021>
- Ma, R., Xu, J., Wang, W., & Lei, J. (2012). The effect of 27 day solar rotation on ionospheric F2 region peak densities (NmF2). *Journal of Geophysical Research*, 117(A3). <https://doi.org/10.1029/2011ja017190>
- Mannucci, A., Wilson, B., Yuan, D., Ho, C., Lindqwister, U., & Runge, T. (1998). A global mapping technique for GPS-derived ionospheric total electron content measurements. *Radio Science*, 33(3), 565–582. <https://doi.org/10.1029/97rs02707>
- Maruyama, T. (2006). Extreme enhancement in total electron content after sunset on 8 November 2004 and its connection with storm enhanced density. *Geophysical Research Letters*, 33(20). <https://doi.org/10.1029/2006gl027367>
- Maruyama, T., Ma, G., & Tsugawa, T. (2013). Storm-induced plasma stream in the low-latitude to midlatitude ionosphere. *Journal of Geophysical Research: Space Physics*, 118(9), 5931–5941. <https://doi.org/10.1002/jgra.50541>
- Matzka, J., Stolle, C., Yamazaki, Y., Bronkalla, O., & Morschhauser, A. (2021). The Geomagnetic Kp index and Derived Indices of Geomagnetic Activity. *Space Weather*, 19(5), e2020SW002641. <https://doi.org/10.1029/2020sw002641>
- Mikhailov, A. V., & Mikhailov, V. V. (1995). A new ionospheric index MF2. *Advances in Space Research*, 15(2), 93–97. [https://doi.org/10.1016/s0273-1177\(99\)80029-5](https://doi.org/10.1016/s0273-1177(99)80029-5)
- Minnis, C., & Bazzard, G. (1960). A monthly ionospheric index of solar activity based on F2-layer ionisation at eleven stations. *Journal of Atmospheric and Terrestrial Physics*, 18(4), 297–305. [https://doi.org/10.1016/0021-9169\(60\)90113-6](https://doi.org/10.1016/0021-9169(60)90113-6)
- Nishioka, M., Tsugawa, T., Jin, H., & Ishii, M. (2017). A new ionospheric storm scale based on TEC and foF2 statistics. *Space Weather*, 15(1), 228–239. <https://doi.org/10.1002/2016sw001536>
- Noll, C. E. (2010). The crustal dynamics data information system: A resource to support scientific analysis using space geodesy. *Advances in Space Research*, 45(12), 1421–1440. <https://doi.org/10.1016/j.asr.2010.01.018>
- Orús, R., Hernández-Pajares, M., Juan, J., & Sanz, J. (2005). Improvement of global ionospheric VTEC maps by using kriging interpolation technique. *Journal of Atmospheric and Solar-Terrestrial Physics*, 67(16), 1598–1609. <https://doi.org/10.1016/j.jastp.2005.07.017>
- Perrone, L., & De Franceschi, G. (1998). Solar, ionospheric and geomagnetic indices. *Annals of Geophysics*, 41(5–6), 843–855. <https://doi.org/10.4401/ag-3824>
- Roma-Dollase, D., Hernández-Pajares, M., Krankowski, A., Kotulak, K., Ghoddousi-Fard, R., Yuan, Y., et al. (2018). Consistency of seven different GNSS global ionospheric mapping techniques during one solar cycle. *Journal of Geodesy*, 92, 691–706. <https://doi.org/10.1007/s00190-017-1088-9>
- Schaer, S., Beutler, G., Rothacher, M., & Springer, T. A. (1996). Daily global ionosphere maps based on GPS carrier phase data routinely produced by the CODE Analysis Center. In *Proceedings of the IGS AC workshop*, Silver Spring, USA, 181–192.
- Schaer, S., Gurtner, W., & Feltens, J. (1998). IONEX: the ionosphere map exchange format version 1. In: *Proceedings of the IGS AC workshop, Germany*, 9.
- Schmölter, E., Berdermann, J., & Codrescu, M. (2021). The delayed ionospheric response to the 27-day solar rotation period analyzed with GOLD and IGS TEC data. *Journal of Geophysical Research: Space Physics*, 126(2), e2020JA028861. <https://doi.org/10.1029/2020ja028861>

- Schreiber, H. (1998). On the periodic variations of geomagnetic activity indices Ap and ap. *Annales Geophysicae*, 16(5), 510–517. <https://doi.org/10.1007/s00585-998-0510-2>
- Sori, T., Shinbori, A., Otsuka, Y., Tsugawa, T., & Nishioka, M. (2019). Characteristics of GNSS total electron content enhancements over the midlatitudes during a geomagnetic storm on 7 and 8 November 2004. *Journal of Geophysical Research: Space Physics*, 124(12), 10376–10394. <https://doi.org/10.1029/2019ja026713>
- Sulaiman, S., Ali, M. A. M., & Yatim, B. (2007). Ionospheric GPS-TEC during the 2004 major storm events at Scott Base station Antarctica. In *2007 IEEE International conference on Telecommunications and Malaysia International conference on Communications* (pp. 289–293). <https://ieeexplore.ieee.org/document/4448648>
- World Data Center for Geomagnetism, Kyoto, Nose, M., Iyemori, T., Sugiura, M., Kamei, T. et al. (2015). *Geomagnetic Dst index*. <https://doi.org/10.17593/14515-74000>
- Yang, H., Monte-Moreno, E., Hernández-Pajares, M., & Roma-Dollase, D. (2021). Real-time interpolation of global ionospheric maps by means of sparse representation. *Journal of Geodesy*, 95, 71. <https://doi.org/10.1007/s00190-021-01525-5>
- Zhang, H., Xu, P., Han, W., Ge, M., & Shi, C. (2013). Eliminating negative VTEC in global ionosphere maps using inequality-constrained least squares. *Advances in Space Research*, 51(6), 988–1000. <https://doi.org/10.1016/j.asr.2012.06.026>